AFRL-ML-WP-TP-2007-404

THE EFFECT OF HARD COATED METALS ON THE THERMO-OXIDATIVE STABILITY OF A BRANCHED PERFLUOROPOLYALKLYETHER LUBRICANT (PREPRINT)

Patrick T. Hellman, Jeffrey S. Zabinski, Lois J. Gschwender, Carl E. Snyder, Jr., and Andras L. Korenyi-Both

OCTOBER 2006

Approved for public release; distribution unlimited.

STINFO COPY

MATERIALS AND MANUFACTURING DIRECTORATE
AIR FORCE RESEARCH LABORATORY
AIR FORCE MATERIEL COMMAND
WRIGHT-PATTERSON AIR FORCE BASE, OH 45433-7750

NOTICE AND SIGNATURE PAGE

AFRL-ML-WP-TP-2007-404 HAS BEEN REVIEWED AND IS APPROVED FOR PUBLICATION IN ACCORDANCE WITH ASSIGNED DISTRIBUTION STATEMENT.

*//Signature//	//Signature//
LOIS J. GSCHWENDER, Program Manager Nonstructural Materials Branch Nonmetallic Materials Division	JEFFREY H. SANDERS, Chief Nonstructural Materials Branch Nonmetallic Materials Division

*Disseminated copies will show "//Signature//" stamped or typed above the signature blocks.

REPORT DOCUMENTATION PAGE

Form Approved
OMB No. 0704-0188

1. REPORT DATE *(DD-MM-YY)*	2. REPORT TYPE	3. DATES COVERED *(From - To)*
October 2006	Journal Article Preprint	

4. TITLE AND SUBTITLE

THE EFFECT OF HARD COATED METALS ON THE THERMO-OXIDATIVE STABILITY OF A BRANCHED PERFLUOROPOLYALKLYETHER LUBRICANT (PREPRINT)

5a. CONTRACT NUMBER
In-house

5b. GRANT NUMBER

5c. PROGRAM ELEMENT NUMBER
62102F

6. AUTHOR(S)

Patrick T. Hellman (University of Dayton Research Institute)
Jeffrey S. Zabinski, Lois J. Gschwender, and Carl E. Snyder, Jr. (AFRL/MLBT)
Andras L. Korenyi-Both (Tribologix)

5d. PROJECT NUMBER
4347

5e. TASK NUMBER
RG

5f. WORK UNIT NUMBER
M06R1000

7. PERFORMING ORGANIZATION NAME(S) AND ADDRESS(ES)

University of Dayton Research Institute
Dayton, OH 45469

Nonstructural Materials Branch (AFRL/MLBT)
Nonmetallic Materials Division
Materials and Manufacturing Directorate
Air Force Research Laboratory, Air Force Materiel Command
Wright-Patterson Air Force Base, OH 45433-7750

Tribologix
Springboro, OH 45066

8. PERFORMING ORGANIZATION REPORT NUMBER
AFRL-ML-WP-TP-2007-404

9. SPONSORING/MONITORING AGENCY NAME(S) AND ADDRESS(ES)

Materials and Manufacturing Directorate
Air Force Research Laboratory
Air Force Materiel Command
Wright-Patterson AFB, OH 45433-7750

10. SPONSORING/MONITORING AGENCY ACRONYM(S)
AFRL-ML-WP

11. SPONSORING/MONITORING AGENCY REPORT NUMBER(S)
AFRL-ML-WP-TP-2007-404

12. DISTRIBUTION/AVAILABILITY STATEMENT
Approved for public release; distribution unlimited.

13. SUPPLEMENTARY NOTES
Journal article submitted to WEAR Magazine.
The U.S. Government is joint author of this work and has the right to use, modify, reproduce, release, perform, display, or disclose the work.
PAO Case Number: AFRL/WS 06-2647, 07 Nov 2006.

14. ABSTRACT

M-50 and carburized Pyrowear 675® steel coupons deposited with commercially available physical vapor deposited (PVD) TiN, TiCN, TiAlCN, TiCrCN/TiB_4C multilayer, electroless Ni (E-Ni) TiN, and E-Ni TiCN coatings were immersed in a branched perfluoropolyalklyether (PFPAE), Krytox AC®, in an oxidative environment at temperatures ranging from 315 to 360°C for a duration of 24 hours and compared to uncoated coupons. Coated and uncoated Pyrowear 675® coupons demonstrated superior corrosion resistance compared to coated and uncoated M-50, respectively. The coatings most resistant to chemical attack in the PFPAE fluid were TiCN, E-Ni TiN, and E-Ni TiCN.

15. SUBJECT TERMS

Oxidation corrosion, perfluoropolyalkylethers, scanning electron microscope, X-Ray photoelectron spectroscopy, solid lubricants, metals

16. SECURITY CLASSIFICATION OF:			17. LIMITATION OF ABSTRACT:	18. NUMBER OF PAGES	19a. NAME OF RESPONSIBLE PERSON (Monitor)
a. REPORT	b. ABSTRACT	c. THIS PAGE			Lois J. Gschwender
Unclassified	Unclassified	Unclassified	SAR	42	19b. TELEPHONE NUMBER *(Include Area Code)* N/A

Standard Form 298 (Rev. 8-98)
Prescribed by ANSI Std. Z39-18

The Effect of Hard Coated Metals on the Thermo-Oxidative Stability of a Branched Perfluoropolyalklyether Lubricant

Patrick T. Hellman
University of Dayton Research Institute
Dayton, Ohio 45469
and
Jeffery S. Zabinski, Lois J. Gschwender*, and Carl E. Snyder Jr.
Air Force Research Laboratory
Wright-Patterson Air Force Base, Ohio 45433
and
Andras L. Korenyi-Both
Tribologix
Springboro, Ohio 45066

*Corresponding author: Lois J. Gschwender
AFRL/MLBT
2941 Hobson Way Bldg 654, Room 136
Wright-Patterson AFB, OH 45433-7750
e-mail: lois.gschwender@wpafb.af.mil
Phone: (937) 255-7530
Fax: (937) 255-2176

Abstract

M-50 and carburized Pyrowear 675® steel coupons deposited with commercially available physical vapor deposited (PVD) TiN, TiCN, TiAlCN, TiCrCN/TiB_4C multilayer, electroless Ni (E-Ni) TiN, and E-Ni TiCN coatings were immersed in a branched perfluoropolyalklyether (PFPAE), Krytox AC®, in an oxidative environment at temperatures ranging from 315 to 360°C for a duration of 24 hours and compared to uncoated coupons. Coated and uncoated Pyrowear 675® coupons demonstrated superior corrosion resistance compared to coated and uncoated M-50, respectively. The coatings most resistant to chemical attack in the PFPAE fluid were TiCN, E-Ni TiN, and E-Ni TiCN.

Key Words

Oxidation Corrosion, Perfluoropolyalkylethers, Scanning Electron Microscope, X-Ray Photoelectron Spectroscopy, Solid Lubricants, Metals

Introduction

Perfluoropolyalkylethers (PFPAEs) are considered good candidates for high temperature liquid lubricant applications due to their exceptional high temperature oxidative stability, excellent viscosity characteristics over large temperature ranges, and commercial availability of linear and branched fluids (1). The problem with using these fluids for high temperature applications is they decompose and cause corrosion in the presence of ferrous and non-ferrous metals and alloys (1-9). Fluid decomposition also occurs in tribological environments at relatively low temperatures in boundary lubrication at asperity contacts. Fluid decomposition in a static high temperature and tribological environments has been proposed to occur by the same two step fluid decomposition mechanism (3,9,10): 1) conversion of the metal surface to a metal fluoride which functions as a Lewis acid site and 2) catalytic decomposition of

the fluid by interaction with these Lewis acid sites. The initial degradation of the PFPAE fluid is due to either high temperatures in a static environment or in a tribological environment at asperity contacts where the localized temperature and shear stresses are at a maximum. One of the principal products of degradation are PFPAE acyl fluorides, which react with metal surfaces to form metal fluoride Lewis acid sites (10,11). These sites autocatalyze the degradation of the PFPAE fluid to form more PFPAE acyl fluorides. Corrosion of the metal surface is also a product of this overall process.

There are three ways to control this decomposition process: enhance the fluid with the use of additives (10,12,13), utilize substrates that minimize the formation of Lewis acid sites, or a combination of the two. Aluminum and ferrous alloys are the most studied substrates with respect to PFPAE research (2-7,14-17). These metals are highly reactive with the PFPAE decomposition products at high temperatures and readily produce aluminum and iron fluorides, respectively. The development of porosity free coating deposition and enhanced metallurgy techniques for stainless steels and other type materials is of the utmost importance to improve the stability of PFPAE lubricants in high temperature environments. To enhance the compatibility of ferrous alloys in the presence of PFPAE lubricants, the amount of iron on the surface can be minimized such as with stainless steels. Stainless steels have a high percentage of chromium (>10%) on the surface that produces a protective oxide layer over the iron. Carbides are also believed to reduce the amount of iron on the surface. Titanium alloys have also been examined in some studies with various conclusions (4,6). Pure titanium is quite compatible with PFPAE fluids, whereas the alloying elements, e.g the aluminum in Ti(6*Al*4V) typically used, are susceptible to attack by PFPAE degradation products.

Recently explored surfaces such as TiN and electroless Ni (E-Ni) have shown improved performance over those previously mentioned (18). One such research effort deposited a TiN coating on a 440C substrate by cathodic arc deposition which was then contacted with a PFPAE lubricant through thermo-oxidation experiments. The post-test coupon surface contained dark raised areas termed as “blisters”. XPS analysis revealed that the blisters were primarily iron fluorides: the product of the ferrous substrate material interaction with the PFPAE lubricant. Beside the blisters were regions of unaffected TiN coating. The proposed failure mechanism stemmed from the cathodic arc deposition process, which is known to produce coatings with pinholes. The porosity of TiN coatings allowed lubricant penetration to the 440C substrate. The interaction of PFPAE lubricant with the 440C surface produced corrosion. This led to an increased specific volume causing coating fracture and exposure of the 440C substrate. The E-Ni coating was found resistant to PFPAE attack at temperatures up to 370°C. This superior performance is attributed to the absence of pinholes in the E-Ni coating. E-Ni coatings are deposited in a solution state method allowing relatively pinhole free coatings to be produced if a proper reducing agent, such as sodium hypophosphite, is used. The use of this reducing agent produces an E-Ni coating with approximately 3 to 15 percent phosphorus (P) depending on the operating conditions (19). Coatings with < 0.05 percent P tend to be porous and with > 10 percent P tend to have continuous impurities (19). Between these values E-Ni is amorphous providing an almost porosity free coating (19). Pure Ni coatings can be deposited, but they result in a highly porous, brittle, and highly stressed coating which provides little or no substrate protection (19).

There has yet to be a single research effort which explores various commercially available coatings. The objective of this effort is twofold: 1) to determine the resistance of a

carburized stainless steel to the attack of a PFPAE lubricant using M-50 steel as a baseline and 2) to determine the resistance of various titanium based coatings to the attack of a PFPAE fluid using M-50 steel and the carburized stainless steel as performance baselines as well as substrates for the coatings.

Experimental

The base fluid used for this study was Krytox® AC, which has the following structure, $CF_3CF_2CF_2O[CF(CF_3)CF_2O]_mCF_2CF_3$. Two ferrous alloys were used as substrates for the coating process: M-50 and carburized Pyrowear 675® stainless steel, which is referred to as CRS for the remainder of this publication. Table 1 displays the composition of both the M-50 and the CRS steel washers. This stainless steel has potential application in gas turbine engine bearings. The CRS coupons were carburized to a 2.3 mm depth. Due to the hardness of CRS, the washers were machined to a thickness of ~5.1 mm compared to ~1.07 mm for the M-50 washers. The coatings investigated were commercially available TiCN, TiN, TiAlCN, TiCrCN/TiB_4C multilayer, E-Ni TiCN, and E-Ni P TiN from several coatings companies. The deposition methods and reasons for their selection are given in Tables 2 and 3, respectively. The two different TiN coatings were obtained from two commercial sources and are designated as "TiN A" and "TiN B". The TiCrCN/TiB_4C multilayer was produced under two different processes by the same commercial source designated as "TiCrCN/TiB_4C A" and "TiCrCN/TiB_4C B". The E-Ni coating was deposited with a P content between 8-12%. A limited number of metal coupons were coated: two M-50 and two CRS for each coating type.

Oxidation-Corrosion

Oxidation-Corrosion (OC) type testing has commonly been used as a way to establish the suitability of candidate lubricants for application in gas turbine engines. Versions of this test are

included in military specifications MIL-PRF-7808 and MIL-PRF-23699 and test method ASTM D 4636. The correlation between a miniaturized OC test and the larger scale ASTM test method was previously completed and reported (2). Although the detailed apparatus description is not given, a summary is provided here. The metal coupon of a known weight was suspended in six mL of fluid for 24 hours. Dry air was bubbled through the fluid at a rate of 1 L/h at temperatures ranging from 315 to 360°C. After the 24 hour test, the coupon was removed, cleaned ultrasonically in solvent, and re-weighed. Post-test analysis included visual inspection, fluid viscosity change, acid number change, fluid weight loss, and coupon weight loss.

The failure criteria are shown in Table 4. Failures are generally caused by excessive coupon weight change or the appearance of particles in the test fluid. The coupon weight change failure criteria, based on the area of the coupon, have been previously established based on experience (2). This allows comparison between coupons with different surface areas.

X-ray Photoelectron Spectroscopy

Post-test surface analysis of the coupons was conducted by X-ray Photoelectron Spectroscopy (XPS). Preceding the analysis the coupons were ultrasonically cleaned three times in 1,1,2 trichlorotrifluoroethane and once in acetone for fifteen minutes each. The XPS spectra were collected by a Surface Science Instruments SSX-100, using monochromatic Al K α X-rays at an energy of 1486.6 eV. All spectra were taken with a 400 x 1000 micron X-ray spot. Ion sputtering used 5 keV Ar^+ ions with a sputtering rate of 0.5 Å/s with a SiO_2/Si standard. All spectra and binding energies were referenced to the C 1s adventitious carbon peak of 284.7 eV.

Scanning Electron Microscope

Scanning Electron Microscope (SEM) micrographs were collected with the Philips XL 30 ESEM using 15 kV. Elemental analysis was performed by Energy Dispersive X-ray Spectroscopy (EDS).

Results and Discussion

Table 5 shows the changes in fluid viscosity and acid number, fluid weight loss, coupon weight change, and fluid appearance after the OC testing for each of the various coupons. The majority of experiment failures occurred due to the presence of particles in the lubricant. For each coupon type, select OC, XPS, SEM, and EDS comments are given in Table 6. Extensive color change was observed at all temperatures for each coating during the post-test OC visual inspection.

Uncoated Steels

OC failure occurred at 345°C for the CRS coupons and 315°C for the M-50 coupons (Tables 5 & 6). SEM micrographs in Figure 1 illustrate the corrosion on the surface of the M-50 coupon. The pre-test coupon was fairly smooth, but the surface of the post-test 315^{o}C coupon had a large amount of blisters. The CRS coupons appeared similar at 345^{o}C. The increased OC stability for the CRS coupons was expected based on the lower iron content compared to M-50 (Table 1). These results were used as a baseline for the coatings results.

TiN A/TiN B

At 330°C, both types of TiN (M-50) failed due to particles in the post-test fluid, whereas those with the CRS substrate passed. Viewing these coupons under various magnifications revealed the previously reported blisters as shown in Figure 2 (18). Elemental analysis with EDS confirmed the blisters consisted largely of iron, fluorine, carbon, and oxygen (Table 7). Directly adjacent to the blisters, titanium, oxygen, and nitrogen were the main elemental components

indicating the coating was intact in non-blister areas. The CRS substrate coupon blisters were smaller then those on coupons using the M-50 substrate as shown in Figure 2. (Note the different scales.) The increased coating fracture seen on the M-50 coupons is a function of M-50's higher reactivity towards the PFPAE degradation products compared to CRS. This is evident by the metal weight change in Table5 for M-50 at 315°C (1.00 mg/cm^2) and CRS at 330°C (0.15 mg/cm^2). To investigate the failure mechanism of these coupons further, XPS analysis was utilized.

Figure 3 shows the unsputtered and sputtered XPS survey spectra and spectral regions for TiN A (CRS). Due to the small size and proximity of the blisters, the XPS spectra in Figure 3 include both areas with and without blisters. The XPS spectra should be viewed as an average surface composition. The maximum intensities of these spectra were normalized to the same value to assist comparison of the spectra shape. The unsputtered surface consisted mostly of fluorine, oxygen, titanium, and some carbon seen in the survey spectra. With brief sputtering most of the residual fluid was removed from the surface. This reduced the relative amounts of fluorine and carbon on the surface and increased the amount of oxygen and titanium. Since the amount of fluorine on the surface decreased greatly after brief ion sputtering, the surface can be considered relatively inert to attack by PFPAE degradation products. The removed fluorine was that of residual physisorbed PFPAE lubricant on the coating surface. The Ti $2p_{3/2\text{-}1/2}$ peak envelope was fitted with two peaks at 459.0 and 464.7 consistent with TiO_2 supporting the assessment that the coating surface was not converted to a fluoride containing surface. After sputtering, the titanium peaks broadened towards the lower binding energies consistent with unstoichiometric TiN_xO_{1-x}. The F 1s region consisted of two peaks at 685.0 and 688.4 eV. The higher binding energy is a result of the physisorbed PFPAE fluid on the surface and the lower

binding energy are iron fluorides detected from the iron blisters. The individual components of the Fe spectra are indistinguishable, such as the oxides from the fluorides which occur around the same binding energies (~711 eV), but based on the F 1s spectra and EDS there was a combination of both on the surface. This supports the hypothesis that the failure mechanism of these coatings is a result of the PFPAE degradation products diffusing through the coating pores and then corroding the substrate. The corroded substrate has an increased specific volume which leads to coating fracture and the formation of the iron blisters (18).

The cathodic arc deposition method (TiN B) inherently has a higher porosity rate than other PVD methods due to the formation of particles during the arc evaporation process, but the molten pool electron beam deposition process (TiN A) still produced a porous coating with regard to PFPAE lubricants.

TiCN

Whereas the TiN (M-50) coupons failed at 330°C due to particles, the TiCN (M-50) passed. The SEM/EDS and XPS results were similar to the TiN coatings: areas of blisters and areas of intact coating, but the TiCN (M-50) coupons had fewer blisters than the TiN (M-50) coupons. Two possible explanations are 1) the TiN coatings have a higher porosity allowing for an increased amount of substrate corrosion and coating cracking and/or 2) various properties such as hardness, adhesion, carbon content, and residual stresses among others prevented the TiCN coating from cracking as much as the TiN coating. These properties greatly affect the effectiveness of a coating and their relations are not completely understood.

TiAlCN

The TiAlCN (M-50) test at 360°C resulted in almost complete degradation of the fluid: approximately 97 percent fluid weight loss. A layer of white particles was present inside the

test-tube and on the air tube. X-Ray Fluorescence (XRF) was performed by Chemsys Incorporated on these particles revealing the presence of aluminum and titanium (Table 8). This partial loss of aluminum from the coating tested at 360°C was confirmed with SEM micrographs (Figure 4), EDS (Table 9), and XPS analysis (Figure 5).

XPS analysis revealed that after brief sputtering the concentration of fluorine on the surface did not decrease substantially for any of the TiAlCN coated coupons at the various temperatures. This shows the majority of the fluorine on the surface was bonded to the coating. This is due to at least partial conversion of the aluminum contained in the coating into an aluminum fluoride since neither TiN nor TiCN had a large amount of fluorine on the surface after sputtering. Also, at the lowest two temperatures, the Al spectra were closely associated with the binding energies of aluminum oxides and fluorides in Figure 5. As the temperature increased, the spectra broadened to the higher binding energies consistent to that of AlF_6^- around 78.0 eV (9).

The F 1s spectra shown in Figure 5 confirm there is a drastic change in how fluorine has interacted with the surface at 360°C. At 315 and 330°C the binding energies, 686.6 and 686.8 eV respectively, and the line shape of the F 1s spectra are similar. Herrera-Fierro assigned the AlF_3 peak to a binding energy of 687.2 eV which is close to what has been reported here (9). At 345°C, the F peak broadened towards the higher binding energies and at 360°C there were two distinct peaks at 684.8 and 688.3 and a slight peak at 692.5 eV. The lowest binding energy was associated with iron fluorides from the iron blisters on the surface. The middle binding energy was from the residual fluid on the coupon (C-F). The highest binding energy was unknown, but was probably the result of a slight amount of surface charging since the coupon surface was not homogenous.

TiAlCN in combination with PFPAE lubricants should not be considered as a suitable coating for high temperature gas turbine engines since the degradation products interacted with the TiAlCN coating to produce aluminum fluorides and when failure did occur, as with the M-50 substrate at 360°C, the corrosion and fluid degradation was severe.

TiCrCN/TiB_4C A and TiCrCN/TiB_4C B

Both A and B coating types displayed similar performance in OC testing and analogous results from XPS and SEM data and therefore are not distinguished in the following text. Only small particles were observed for the failures of the TiCrCN/TiB_4C (CRS) coupons as opposed to particles and flakes for the M-50 substrate coupons. The flakes were not only present in the fluid; the coating was visually separated from the coupon at various locations (Figure 6). This behavior was not observed for the coated CRS coupons. As expected, the M-50 coupons displayed large areas of iron blisters causing the flaking of the coating shown in Figure 6. The XPS survey spectra for both A and B type TiCrCN/TiB_4C coated coupons contained well formed iron features compared to the previous coatings, an indication of an increased amount of iron blistering that occurred with this coating.

Since the CRS substrate coupons did not flake like the M-50 substrate coupons, neither 1) the difference of the coefficients of thermal expansion (COTE) of the two coating layers (TiCrCN and TiB_4C) or 2) fluid reaction with an element in the coating are believed to be the major cause of the coating failure. If the difference of the COTE or a fluid coating reaction were the major failure mechanisms then the coating would have acted the same regardless of the substrate used.

At 360°C, both types of TiCrCN/TiB_4C (M-50) failed due to particles/flakes and fluid weight loss. The fluid weight losses from these coatings at this temperature were a staggering

39% and 33%. The negative viscosity change coupled with the large fluid weight loss indicates that the degradation process involved PFPAE fluid chain scission. Before the ultrasonic cleaning, flakes were observed in the fluid and on the metal. During the cleaning a large amount of brownish flakes materialized (Figure 6). It appeared as through the coating was completely removed from the metal surface. XPS supported this assessment revealing that the atom percent of titanium on the coupon surface was less than one percent and there was a high percent of iron. SEM micrographs coupled with EDS confirm that the surface is mostly iron as shown in Figure 7.

The coating failed due to cracking caused by iron blisters. At this juncture, the suitability of a TiCrCN/TiB_4C coating preventing PFPAE decomposition is limited due to the porosity of the coating.

E-Ni TiN

No iron blisters were detected using high resolution SEM techniques for any of these coupons. Both the 360°C M-50 and CRS substrate coupons had areas where the TiN coating delaminated from the E-Ni P surface (Figure 8). The cause of this is unknown since E-Ni surfaces tend to be a good adhesion surface for other coatings (18). There was a small amount of F detected with EDS in both Ti and Ni regions (Table 10). As with the TiN coatings, after light sputtering, the amount of fluorine was drastically reduced revealing that fluorine was not directly bonded to the surface in large amounts for either the Ti or the Ni regions. the fluorine was the result of physisorbed PFPAE fluid.

E-Ni TiCN

Both the M-50 and CRS substrate coupons performed acceptably at 360°C. This is the only coating to perform this well in the OC testing. No iron blisters were detected using high

resolution SEM techniques for any of these coupons as shown in Figure 9. The TiCN coating remained intact for both the M-50 and CRS substrates. As with the TiN coatings, after light sputtering, the amount of fluorine was drastically reduced revealing that fluorine was not directly bonded to the surface in large amounts for either the Ti or the Ni regions. The surface was heavily oxidized compared to pre-test coupons as shown in Table 11.

Conclusions/Recommendations

1. Uncoated CRS coupons demonstrated superior OC performance compared to uncoated M-50 coupons. The lower levels of iron in the CRS compared to M-50 resulted in inhibition of the corrosion process.
2. Coated coupons have been found to fail by three different mechanisms: 1) chemical reaction of the PFPAE fluid degradation products with a reactive element in the coating, e.g., Al; 2) fluid degradation products reaching the more reactive metal substrates through the porosity of a coating; 3) delamination of the coating, e.g. delamination of TiN from E-Ni P.
3. The TiN, TiCN, and TiCrCN/TiB_4C multilayer coatings had iron blisters present at all temperatures tested. This is most likely due to the PFPAE degradation products diffusing through the porous coating and corroding the substrate creating a difference in specific volume. This caused the coating to crack.
4. Both of the different deposition methods for the TiN coating yielded iron blisters. The cathodic arc method coupons contained more iron blisters than the molten pool electron beam method coupons.
5. The TiAlCN coating interacted readily with the PFPAE lubricant at all the temperatures tested producing an aluminum fluoride surface. At the highest temperature tested, iron blisters were present.

6. E-Ni TiN and E-Ni TiCN coatings performed better than their counter parts, TiN and TiCN respectively. The E-Ni P coating prevented the formation of the iron blisters.
7. TiCN, E-Ni TiN, and E-Ni TiCN coatings demonstrated superior performance in oxidation corrosion testing.
8. Further research in regard to E-Ni P should be performed to determine the extent of protection it offers. Various PFPAE fluid applications may immediately benefit from the implementation of this coating.
9. Improvement in the deposition process for coatings needs to be investigated for both TiN and TiCN which have been shown to be relatively inert to PFPAE degradation products, but the porosity of these coatings is their limiting factor.
10. Although not a part of this study, based on the literature review, additives for PFPAEs are expected to be highly effective when used in conjunction with coatings to passivate the entire system using a PFPAE lubricant.

Acknowledgements

The authors would like to acknowledge Angela Campo and Ben Phillips of Air Force Research Laboratory and Dr. Peter John and Bill Ragland of UDRI for their beneficial discussions.

References

(1) Snyder, C.E. Jr., Dolle, R.E. Jr. Development of Polyperfluoroalkylethers as High Temperature Lubricants and Hydraulic Fluids. *ASLE Trans*. 1976; **19**: 171-180.

(2) Gschwender, L., Snyder, C.E., Fultz, G.W., Hahn, D.A., and Demers, J.R. Characterization of Model Perfluoropolyalkylethers by Miniaturized Thermal Oxidative Techniques-Part I: Modified Oxidation-Corrosion Test. *Trib. Trans*. 1995; **38**: 618-626.

(3) Kasai, P.H. Perfluoropolyethers: Intramolecular Disproportionation. *Macromolecules*. 1992; **25**: 6791-6799.

(4) Gschwender, L.J., and Snyder C.E. Jr. High Temperature Oxidative Stability of $C_3F_7O[CF(CF_3)CF_2O]_xC_3F_7$ and $CF_3(OCF_2CF_2CF_2)_yCF_3$ Perfluoropolyalkylethers and Formulations in the Presence of Metals. *Lub. Eng.* 2000; **56**: 17-22.

(5) Keller, M.A., and Saba, C.S. Catalytic Degradation of a Perfluoroalkylether in a Thermogravimetric Analyzer. *Trib. Trans.* 1998; **41**: 519-524.

(6) Paciorek, K.J.L., Masuda, S.R., Lin W., and Jones, W.R. Jr. Effect of Metal Alloys, Degradation Inhibitors, Temperatures, and Exposure Duration on the Stability of Poly(hexafluoropropene oxide) Fluid. *Ind. Eng. Chem. Res.* 1997; **36**: 2859-2861.

(7) Hayashida, K. Yamamoto, K., and Nishimura, M. Wear and Degradation Characteristics of Perfluoroalkylpolythers (PFPEs) in High Vacuum. *Trib. Trans.* 1994; **37**: 196-200.

(8) Trivedi, H.K., and Saba, C.S. Effect of Temperature on Tribological Performance of a Silicon Nitride Ball Material with a Linear Perfluoropolyalkylether. *Trib. Letters*. 2001; **10**: 171-177.

(9) Herrera-Fierro, P., Jones, W.R. Jr., and Pepper, S.V. Interfacial Chemistry of a Perfluoropolyether Lubricant Studied by X-Ray Photoelectron Spectroscopy and Temperature Desorption Spectroscopy. *J. Vac. Sci. Technol.* 1993; **11**: 354-367.

(10) Zehe, M.J., and Faut, O.D. Acidic Attack of Perfluorinated Alkyl Ether Lubricant Molecules by Metal Oxides Surfaces. *Trib. Trans.* 1990; **33**: 634-640.

(11) John, P.J. and Liang, J. Initial Metal Fluoride Formation at Metal/Fluorocarbon Interfaces. *J. Vac. Sci. Technol.* 1994; **12**: 199-203.

(12) John, P.J., Liang, J., and Cutler, J.N. Surface Activity of High-Temperature Perfluoropolyalkylether Oil Additives. *Trib. Letters*. 1998; **4**: 277-285.

(13) Demers, J.R., Gschwender, L.J., and Snyder, C.E. A New Technique for the Investigation of Liquid Lubricant Degradation: The Oxidation Corrosion Conductivity Test. *Lub. Eng.* 1994; **51**: 321-327.

(14) Nakayama, K., Dekura, T., Kobayashi, T. Effect of Additives on Friction, Wear, and Iron Fluoride Formation under Perfluoropolyether Fluid Lubrication in Vacuum and Various Atmospheres Containing Oxygen. *Wear*. 1996; **192**: 178-185.

(15) Sanders, J.H., Cutler, J.N., and John, G. Characterization of Surface Layers on M-50 Steel Exposed to Perfluoropolyalkylethers at Elevated Temperatures. *App. Sur. Sci.* 1998; **135**: 169-177.

(16) Paciorek, K.J.L., Masuda, S.R., Lin, W.-H., and Nakahara, J.H. Thermal Oxidative Stability of Perfluoropolyalkylethers and Development of Quantitative Structure-Stability Relationships. *Jour. Fluorine Chem.* 1996; **76**: 21-27.

(17) Paciorek, K.J.L., Kratzer, R.H., Kaufman, J., and Nakahara, J.H. Thermal Oxidative Studies of Poly(hexafluoropropene Oxide) Fluids. *J. App. Polym. Sci.* 1979; **24**: 1397-1411.

(18) Zabinski, J.S. and Voevodin, A.A. Recent Developments in the Design, Deposition, and Processing of Hard Coatings. *J. Vac. Sci. Technol.* 1998; **16**: 1890-1900.
(19) Bhushan, B., and Gupta, B.K. Handbook of Tribology: Materials, Coatings, and Surface Treatments. McGraw-Hill, Inc., New York 1991.

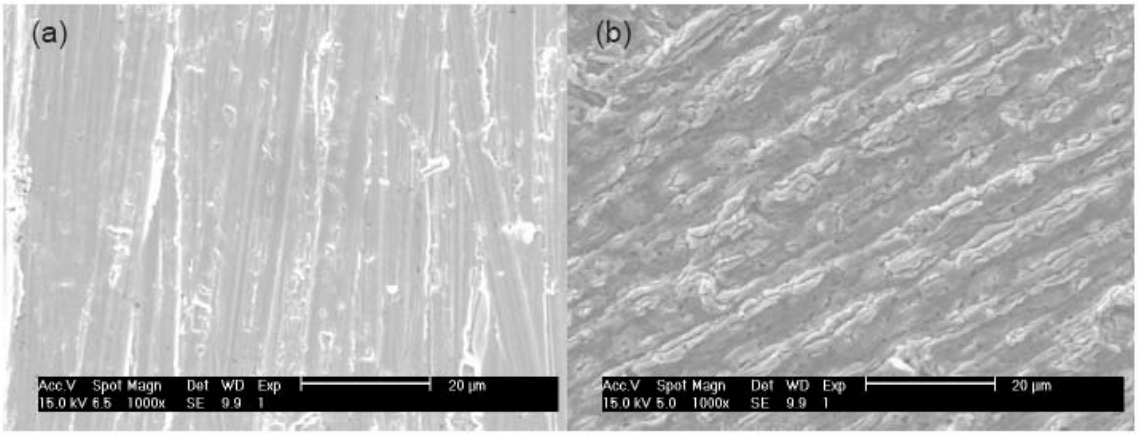

Figure 1: SEM Micrographs of M-50 (a) Pre-test; (b) Post-test

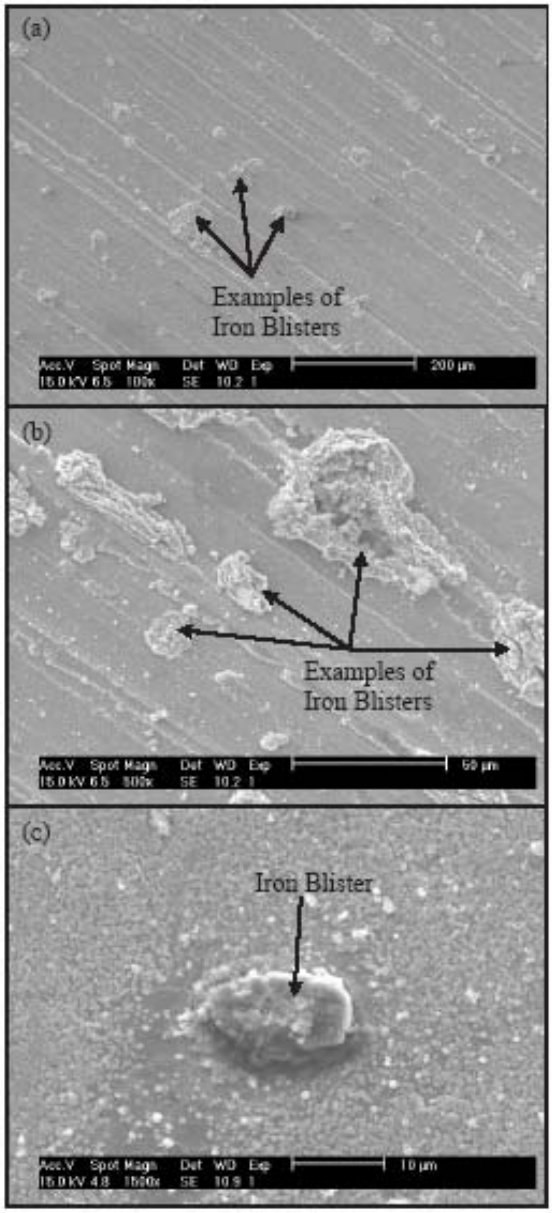

Figure 2: SEM Micrographs of TiN A 330°C OC Coupons

(a) TiN A (M-50); (b) TiN A (M-50); (c) TiN A (CRS)

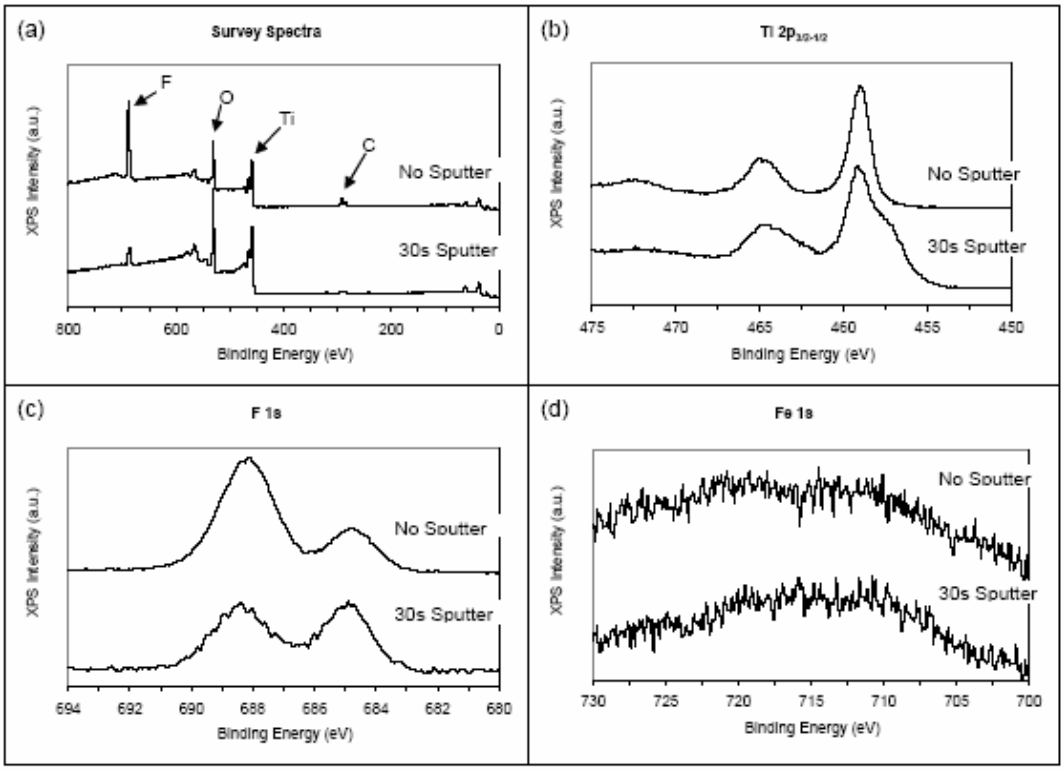

Figure 3: Select XPS Spectra for the TiN A (CRS) Coupon

(a) Survey Spectra;(b) Ti $2p_{3/2\text{-}1/2}$; (c) F 1s; (d) Fe 1s

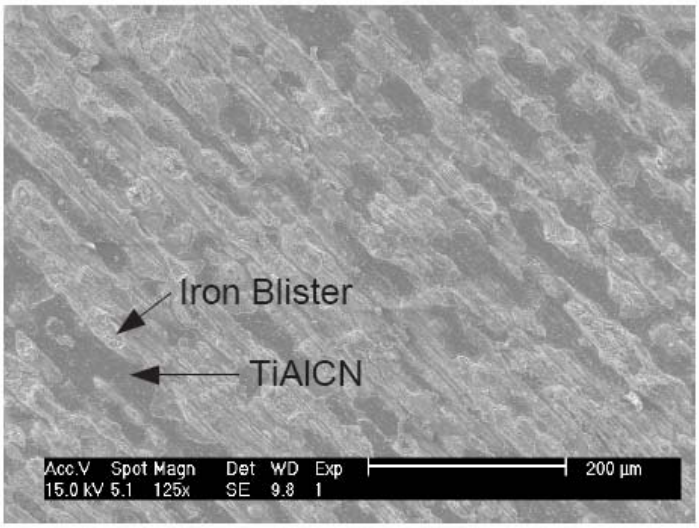

Figure 4: SEM Micrograph of the 360°C OC TiAlCN (M-50) Coupon
(Light Area-Fe Blisters; Dark Area-Coating)

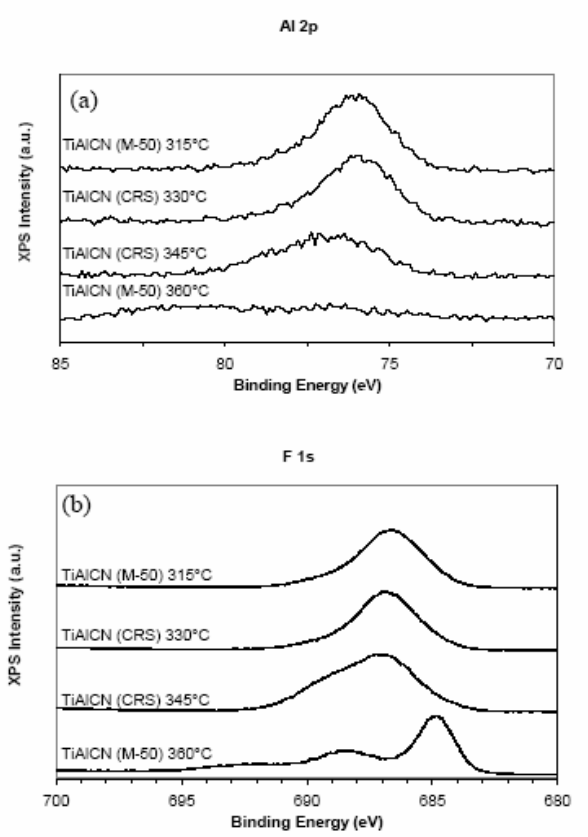

Figure 5: Select XPS Spectra Regions for TiAlCN Coupons (a) Al 2p spectra region; (b) F 1s spectra region after 30s of sputtering

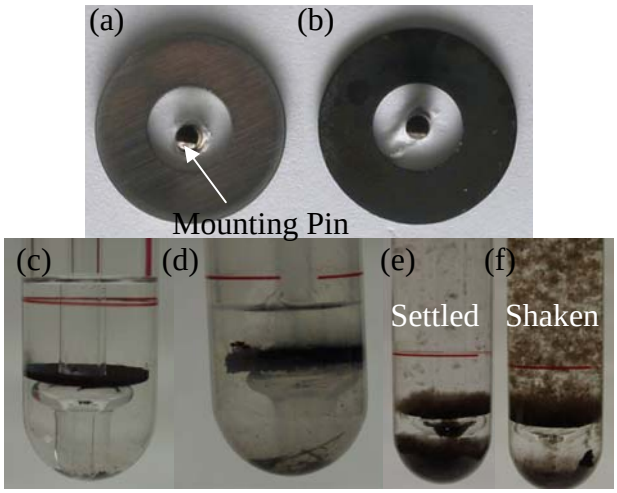

Figure 6: TiCrCN (M-50) 360°C OC Pictures (a) Pre-Test coupon (b) 360°C Post-Test coupon after ultrasonic cleaning in solvent (c) 330°C Post-test OC apparatus and coupon (d) 360°C Post-Test OC apparatus and coupon (e) and (f) 360°C Post-Test OC apparatus and coupon after ultrasonic cleaning in solvent

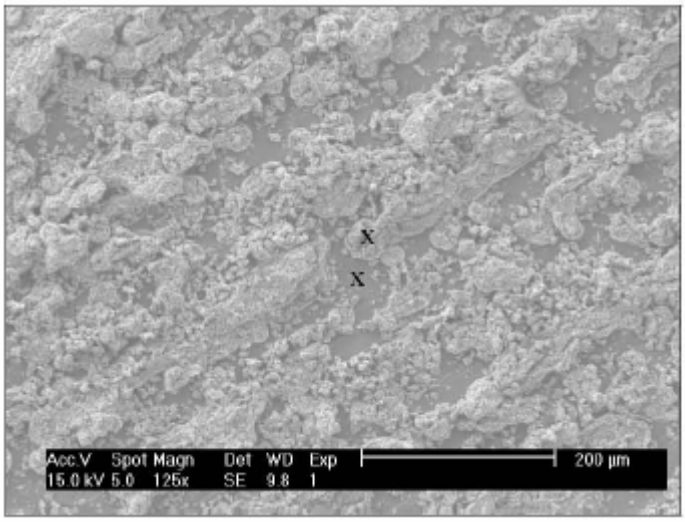

Element	Blister (at.%)	Beside Blister (at%)
C	9.7	5.7
N	-	37.7
O	25.8	8.7
F	36.7	13.1
Ti	<1	20.9
Mo	1.5	-
V	<1	-
Cr	1.8	10.9
Fe	22.6	3.1

Figure 7: SEM Micrograph and EDS Compositions of the TiCrCN (M-50) A 330°C Coupon

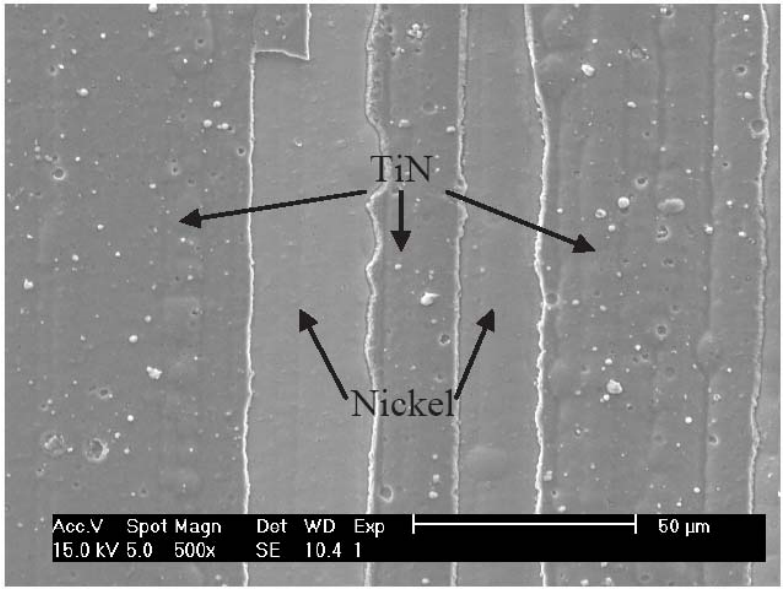

Figure 8: SEM micrograph of the 360°C E-Ni TiN (M-50) Coupon

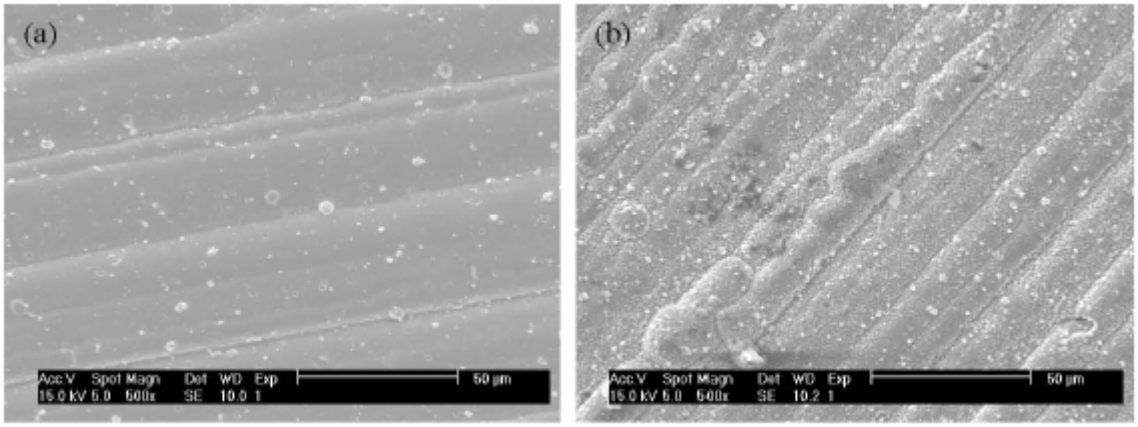

Figure 9: SEM Micrographs of (a) Pretest E-Ni TiCN Coupon and (b) Post-test E-Ni TiCN (M-50) 360°C Coupon

Table 1: Composition of M-50 and CRS Steels

	% Composition	
Element	M-50	CRS
Carbon	0.80-0.85	0.07
Manganese	0.15-0.35	0.65
Silicone	0.10-0.25	0.40
Phosphorous	0.00-0.015	-
Chromium	4.00-4.25	13.00
Molybdenum	4.00-4.50	1.80
Vanadium	0.90-1.10	0.60
Nickel	0.15 Max	2.60
Cobalt	0.25 Max	5.40
Tungsten	0.25 Max	-
Copper	0.10 Max	-
Iron	87.94-90.05	75.48

Table 2: Coating Deposition Methods

Coating Type	Deposition Method
TiN A	Molten Pool Electron Beam Deposition
TiN B	Cathodic Arc Ion Plating
TiCN	Cathodic Arc Ion Plating
TiAlCN	Cathodic Arc Ion Plating
TiCrCN/TiB_4C	TiCrCN by Cathodic Arc Ion Plating — TiB_4C by Sputtering (performed in the same chamber)
E-Ni TiN	Electroless Deposition of Nickel followed by Cathodic Arc Ion Plating of TiCN
E-Ni TiCN	Electroless Deposition of Nickel followed by Cathodic Arc Ion Plating of TiN

Table 3: Coating Selection Reasons

Coating Type	Reason for Selection
TiN	TiN coatings have previously demostrated realitive inertness with PFPAEs in a thermo-oxidative enviroment (18)
TiCN	C increases the hardness and has a lower friction coefficient than TiN
TiAlCN	Al provides an oxide barrier allowing the coating to operate at higher temperatures than TiN or TiCN
TiCrCN/TiB_4C	Cr provides an oxide barrier similiar to that in stainless steels Multilayer coatings tend to minimize porosity
E-Ni P	Has previously demostrated realitive inertness with PFPAEs at least up to 370°C in a thermo-oxidative enviroment Provides a good adhesion surface for other coatings (18)

Table 4: Oxidation-Corrosion Stability Requirements

Viscosity Change	< 20%
Fluid Weight Loss	< 10%
Absolute Metal Weight Change (mg/cm^2)	pass rating < 0.2 0.2 > moderate rating > 0.5 fail rating > 0.5
Particles in Fluid	fail

Table 5: Coatings, CRS, and M-50 Oxidation-Corrosion Results

Table 3: Coatings, CRS, and M-50 Oxidation-Corrosion Results						
TEST TEMP °C	COATING (Substrate)	% VIS CHG @ 40°C	ACID NUMBER CHANGE, mgKOH/g	FLUID % WT. LOSS	METAL WEIGHT CHANGE(mg/cm²)	FLUID APPEARANCE
315	TiAlCN (M-50)	10.81	0.00	6.54	-0.08	no change
315	M-50	5.62	0.00	5.62	1.00**	no change
330	TiN A (M-50)	9.61	0.13	5.00	-0.23*	fluid clear - particles observed**
330	TiN A (CRS)	10.64	0.14	4.00	0.09	no change
330	TiN B (M-50)	8.72	0.12	5.50	-0.32*	fluid clear - particles observed**
330	TiN B (CRS)	11.43	0.12	5.21	0.08	no change
330	TiCN (CRS)	12.84	0.00	5.45	0.11	no change
330	TiAlCN (CRS)	12.19	0.10	5.45	0.05	no change
330	TiCrCN A (M-50)	10.53	0.15	7.22	1.07**	fluid clear - particles/flakes observed**
330	TiCrCN A (CRS)	11.93	0.13	4.90	0.18	no change
330	TiCrCN B (M-50)	6.83	0.13	6.00	-1.26**	fluid clear - particles/flakes observed**
330	TiCrCN B (CRS)	11.24	0.14	5.21	0.20	no change
330	CRS	10.17	0.08	6.06	0.15	no change
345	TiN A (CRS)	11.28	0.14	3.41	-0.01	fluid clear - particles observed**
345	TiN B (CRS)	11.05	0.15	5.00	-0.18	fluid clear - particles observed**
345	TiCN (M-50)	13.70	0.08	7.62	-0.52**	fluid clear - particles observed**
345	TiCN (CRS)	11.41	0.08	6.42	0.04	no change
345	TiAlCN (CRS)	11.71	0.10	7.22	0.13	no change
345	TiCrCN A (CRS)	10.82	0.14	2.94	0.07	fluid clear - particles observed**
345	TiCrCN B (CRS)	10.37	0.06	5.26	0.47*	fluid clear - particles observed**
345	E-Ni TiN (CRS)	10.18	0.14	5.43	0.15	no change
345	E-Ni TiCN (CRS)	10.66	0.14	4.85	0.22*	no change
345	CRS	11.52	0.08	5.31	-0.30*	fluid clear - during ultrasonic cleaning particles observed**
360	TiN A (M-50)	10.57	0.22	8.08	2.12**	fluid clear - particles observed**
360	TiN B (M-50)	6.59	0.22	6.42	1.47**	fluid clear - particles observed**
360	TiCN (M-50)	13.84	0.17	9.38	0.65**	fluid clear - particles observed**
360	TiAlCN (M-50)	no data	no data	97.08**	-1.39**	fluid clear - during ultrasonic cleaning particles observed - fluid does not cover metal - white particles on air tube **
360	TiCrCN A (M-50)	-25.93**	0.14	39.00**	-21.16**	fluid clear - particles observed - clear film like flakes observed**
360	TiCrCN B (M-50)	-7.79	0.13	33.91**	-19.94**	fluid clear - particles observed - clear film like flakes observed**
360	E-Ni TiN (M-50)	12.28	0.11	5.77	-0.60**	fluid clear - particles observed**
360	E-Ni TiN (CRS)	11.27	0.25	5.56	-0.26*	fluid clear - during ultrasonic cleaning particles observed**
360	E-Ni TiCN (M-50)	10.81	0.13	5.66	-0.05	no change
360	E-Ni TiCN (CRS)	10.01	0.13	6.60	0.22*	no change
(24 Hours, 1 Liter air/hour, 6 mL fluid; * Moderate metal weight change rating, ** Failure rating for that specific criterion)						
= Experiment Failure						

Table 6: Select Comments from XPS, SEM, and OC Analysis

Coating	Substrate	Comments
—	M-50	Blisters cover surface at all temperatures; O-C failure at 315°C
—	CRS	Blisters cover surface at all temperatures; O-C failure at 345°C
TiN A&B	M-50	Areas of intact coating and others of blisters; Particles present at 330°C
TiN A&B	CRS	Areas of intact coating and others of blisters; No particles present at 330°C
TiCN B	M-50	Areas of intact coating and others of blisters; Particles present at 345°C
TiCN B	CRS	Areas of intact coating and others of blisters; No particles present at 345°C
TiAlCN	M-50	No blisters except at 360°C; Fluid completely dregraded at 360°C; Aluminum fluoride surface formed at all test temperatures
TiAlCN	CRS	No blisters; Aluminum fluoride surface formed at all test temperatures
TiCrCN A&B	M-50	Blisters at 330°C; Coating completely delaminated from substrate at 360°C
TiCrCN A&B	CRS	Blisters formed at all test temperatures; Particles present at 345°C
E-Ni P TiN	M-50	No blisters at any temperature; TiN delaminated from E-Ni P at 360°C
E-Ni P TiN	CRS	No blisters at any temperature; Particles present at 360°C
E-Ni P TiCN	M-50	No blisters at any temperature; Passed OC test at 360°C
E-Ni P TiCN	CRS	No blisters at any temperature; Passed OC test at 360°C

Table 7: EDS Compositions for the 330°C OC TiN A (M-50) Coupon

Element	Beside Blister (at. %)	Iron Blister (at.%)	Clean M-50 (at.%)
C	4.5	18.3	16.5
N	14.2	<1.0	-
O	39.1	27.5	6.0
F	2.8	17.8	-
Ti	39.4	1.0	-
Si	-	<1.0	1.4
Mo	-	<1.0	2.2
V	-	<1.0	1.0
Cr	-	1.5	3.8
Mn	-	<1.0	<1.0
Fe	-	32.4	68.6

Table 8: XRF Results of the Analysis of the White Particles from the TiAlCN(M-50) OC Experiment at 360°C

Element	rel wt. %
Na	22
Al	42
K	26
Ca	2
Ti	8
Fe	1
Zr	0.1

Table 9: EDS Compositions for the 360°C OC TiAlCN (M-50) Coupon

Element	Beside Blister (at. %)	Iron Blister (at.%)
C	7.5	26.0
N	-	-
O	17.6	16.2
F	45.6	39.9
Al	11.4	-
Ti	16.0	1.8
Mo	-	0.8
Cr	-	2.7
Fe	1.8	12.6

Table 10: EDS of TiN and Ni Regions of the E-Ni TiN 360°C (M-50) Coupon

Element	Ni Region (at. %)	TiN Region (at%)
C	12.3	4.1
N	-	13.2
O	3.5	46.6
F	4.1	3.0
Ti	2.9	33.2
Ni	77.1	-

Table 11: EDS of the Pretest E-Ni TiCN Coupon and Post-test E-Ni TiCN (M-50) 360°C Coupon

Element	Pre-test Coupon (at. %)	Post-test Coupon (at%)
C	29.8	6.6
N	23.2	3.5
O	0.8	49.3
F	-	4.3
Ti	46.2	36.3